第35卷 第3期 焊 接 学 报 Vol. 35 No. 3
2014年3月 TRANSACTIONS OF THE CHINA WELDING INSTITUTION March 2014

基于弧控制的等离子切割电源新型复合控制策略

孙 强， 陈 龙， 陈桂涛， 王华民
(西安理工大学 自动化与信息工程学院，西安 710048)

摘 要：根据非高频引弧技术在等离子切割电源中的应用，分析了等离子电弧的静态特性，推导出了等离子电弧数学模型，并结合电源在非高频引弧、弧转移及弧能量突变过程中的控制需求. 提出了一种新型复合控制策略，该策略的内环是由前馈补偿的电弧电压与反馈电弧电压构成电压闭环复合控制，外环则以电流闭环对等离子弧柱能量进行控制，形成了一种前馈补偿双闭环复合控制方式，以满足电源在非高频引弧负载条件下对快速性和稳定性的控制需求. 结果表明，文中所提控制策略不仅可以提高系统的快速性和鲁棒性，还具有优异的动态响应能力，电源的非线性适应能力强，有效的解决了等离子切割电源的控制需求.

关键词：等离子切割电源；弧控制；前馈补偿；前馈补偿双闭环复合控制
中图分类号：TG483 **文献标识码**：A **文章编号**：0253－360X(2014)03－0071－05

0 序 言

等离子切割电源引弧方式普遍采用高频引弧技术，高频引弧技术具有高引弧率的特点，但高频引弧无法避免高频高压造成的电磁干扰，非高频引弧技术的提出有效的解决了电磁干扰问题[1,2]. 非高频引弧是在压缩气体作用下拉弧，突加气体时若控制不佳，则电弧难以形成或稳定[3]；然而电弧的稳定性直接影响着切割效果，因此对等离子电弧特性及等离子弧控制方法的研究十分必要.

切割电源控制方式目前主要以单环控制为主，一般为电流(或电压)单闭环、电流闭环电压开环切换控制[4－6]. 文献[4]为了解决切割电源的非线性和时变问题采用电压单环控制，由于切割电流直接影响切割质量，电压环的控制不能及时响应电流的控制要求；文献[5]采用电流闭环电压开环切换控制，采用双环切换控制时换点设置困难，并且引弧瞬间的强干扰容易造成控制器在电压电流两个环之间来回切换，导致电路不能正常起弧. 文献[6]提出带指令电流前馈的电流外环电压内环的双闭环控制方式，这种控制方式具有较强的非线性负载适应能力，同时电流环具有较好的稳定性和动态性能，但是电压环的动态性能并不明显，适用于高频引弧，在非高频引弧中存在一定的局限性.

为了解决非高频引弧技术在切割电源中的控制问题，文中提出一种基于弧控制的新型双闭环复合控制策略，通过分析电弧特性及电弧稳定性，推导出非线性等离子电弧数学模型，设计了内环以电弧电压前馈补偿结合电弧电压反馈构成电压闭环，以电流闭环为外环对等离子弧柱能量进行控制，形成一种前馈补偿双闭环复合控制. 所提的新型双闭环复合控制策略不仅保持文献[6]中良好的稳定性和较强的非线性负载适应能力，同时设计的电压环补偿能快速跟随输出电压的动态性能，保证了弧柱电压的稳定性，实现高引弧率，解决了非高频引弧难的困扰，十分适用于大功率非高频引弧的控制.

1 新型控制策略的提出

根据等离子切割工艺需求，在气路打开时，短路电流要在压缩空气、机械、热、电磁共同作用下能成功拉弧必须具备快速性，同时弧柱电压的稳定程度影响着非转移弧的稳定性，此过程的非转移弧产生于喷嘴与电极之间. 材料切割时，将非转移弧转换为转移弧，此过程的转移弧则形成于工件与电极之间，装置检测到切割回路电流大于一定阈值时断开引弧信号，在维持电流恒定的情况下转移电弧，这对于系统的快速性和稳定性要求十分的苛刻，如果控制不佳会直接导致断弧[7]. 在起弧到成功形成转移弧过程中由于等离子电弧在热和电磁的作用下具备非线性和时变的特点，因此对电弧及系统的整体控制十分的严格. 成功完成弧转移后，则是切割过程，在不同切割模式(普通切割、网格和气刨)下必须维

收稿日期：2012－11－06
基金项目：陕西省教育厅产业化培育项目(2011JG08)；陕西省科技厅产科技攻关项目(2011K09－05)

持电弧电流的恒定，才能维持切割表面光滑，保证切割质量和切割效果. 因此文中提出了一种基于弧控制的新型复合控制策略.

1.1 等离子电弧数学模型推导

等离子电弧受电磁场、温度场及热场的影响存在非线性和时变的现象. 为了保证电弧稳定燃烧及切割参数的稳定，必须满足电弧的稳定性要求，根据电弧静特性曲线 $u_1 = f_1(i)$ 和电源外特性曲线 $u_2 = f_2(i)$ 来分析电弧稳定性，图 1 为电源—电弧伏安特性曲线.

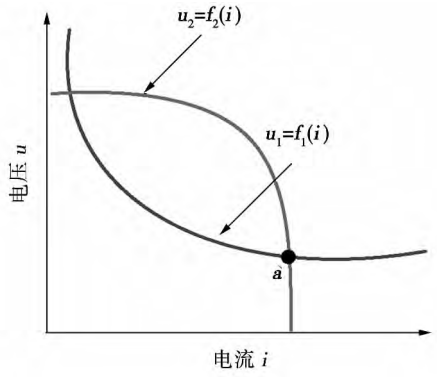

图 1 图 1 电源—电弧伏安特性曲线

Fig. 1 Current-voltage characteristics curve of power-arc

曲线相交点 a 必须满足 $K_w = \left(\frac{\partial u_1}{\partial i} - \frac{\partial u_2}{\partial i}\right)_{i_a} > 0$ 才能达到电弧的平衡点稳定条件. 文献 [8－10] 的电弧质量和能量积分守恒方程，即

$$\int_0^{r_n} \rho c 2\pi r \mathrm{d}r = q_m \tag{1}$$

$$\int_0^{r_n} \rho c h 2\pi r \mathrm{d}r = UI \tag{2}$$

式中：ρ 为等离子弧的质量密度；c 为声速；h 为热焓；U 为喷嘴出口处电弧电压；I 为喷嘴出口处电弧电流；r 为喷嘴径向坐标；r_n 为喷嘴半径；q_m 为离子气在喷嘴出口处的质量流速率[5].

根据文献 [8－10]，在气路压力为 0.1 ~ 1.0 MPa 范围内，ρc，ρch 正比于压力 p. 因此根据双区域电弧模型，将式(1)，式(2)简化为

$$p[K_{1a}A_a + K_{1o}(A_n - A_a)] = q_m \tag{3}$$

$$p[K_{2a}A_a + K_{2o}(A_n - A_a)] = UI \tag{4}$$

式中：A_a 为弧柱截面积；A_n 为喷嘴截面积；K_{1a} 和 K_{2a} 为内部高温区系数；K_{1o} 和 K_{2o} 为外部低温区系数.

使用 T100 喷枪，直径 $d_r = 2.4$ mm，根据式(1)～式(4)以气压、弧柱电压及弧柱电流作为参数变量对电弧模拟曲线进行仿真[9]，如图 2 所示. 根据模拟电弧曲线，采用非线性曲线拟合方法对电弧进行逼近处理，假设电弧方程为

$$U = a_1/I + b_1 e^{(-c_1 I)} \tag{5}$$

如图 3 所示，采用非线性最小二乘法对电弧模拟曲线进行拟合处理，得到的等离子电弧模拟曲线和拟合曲线伏安特性曲线，其中拟合系数 $a_1 = 1\ 075$，$b_1 = 34.324\ 9$，$c_1 = 0.002\ 4$. 求取的等离子电弧等效阻抗数学模型为

$$Z_0 = a_1/I^2 + b_1 e^{(-c_1 I)}/I \tag{6}$$

进而得到电弧补偿环节，即

$$G_{f_1}(s) = Z_0 \tag{7}$$

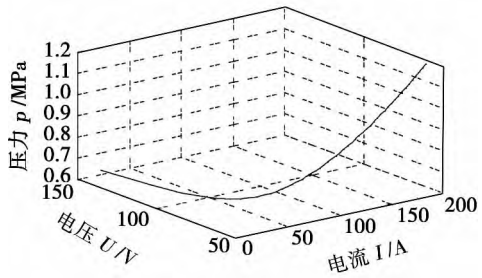

图 2 等离子切割电弧模拟曲线

Fig. 2 Cutting plasma arc simulation curve

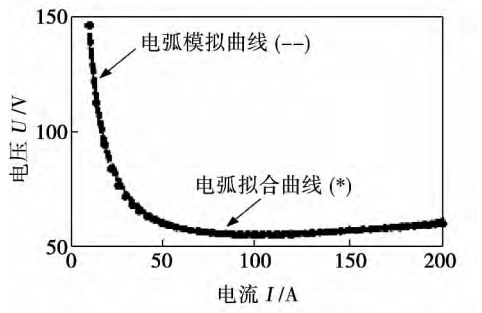

图 3 等离子切割电弧伏安特性曲线

Fig. 3 Current-voltage characteristics of cutting plasma arc

1.2 新型双闭环复合控制策略的设计

根据文献 [11]，用一阶惯性环节去近似模拟传统方法的三角载波电流控制逆变器的频率特性存在一定的误差，而采用前馈补偿的方法设计的三角载波逆变器可减小误差且具有很好的跟踪能力. 因此文中基于半桥结构采用给定扰动预先补偿的原理，在反馈控制的基础上增加前馈控制，对给定的扰动(图 4 中 I_{ref} 和 u_0)采取预先补偿措施，当扰动出现但未来得及影响到被控量时，前馈控制作用就产生了，这样在电弧不稳定时，系统能快速补偿，使电弧仍然保持稳定. 因此前馈补偿比纯反馈控制更为及时且不受系统延迟的影响，这样系统的输出电流能快速跟踪指令电流 I_{ref}，而前馈控制通常不单独使

用,应该与反馈控制相结合构建复合控制[12],利用反馈作用最终消除跟踪产生的误差,新型半桥三角载波电流控制框图如图 4 所示. 当电源输出电流为 i_0 时,若能有效的快速跟踪给定电流 I_{ref},则有 $I_{ref}=i_0$,此时系统能够无误差跟踪给定电流,所以电压环误差输出的 Laplace 方程表达式为

$$u_e(s)=I_{ref}G_f(s)-u_0(s) \tag{8}$$

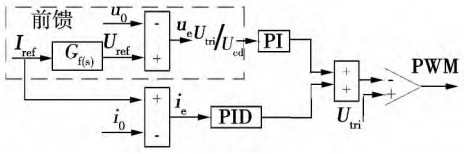

图 4　新型半桥三角载波电流控制框图

Fig. 4　Novel triangular carrier control block of half bridge

半桥拓扑主要受 u_0 和输出阻抗的扰动影响,而三角载波控制的半桥拓扑可近似为一个比例系数 U_{tri}/U_{cd},因此可设计一个三角载波控制比例补偿系数 U_{cd}/U_{tri}; 负载阻抗的扰动则用电弧模型进行补偿,进而实现电压环的补偿设计.

由于电流直接影响切割质量,在保证一定的切割能力和弧的快速性基础上以电流为内环; 而在起弧过程中对弧柱电压的控制利于电弧的稳定燃烧并且保证弧的稳定性,因此设计了一种以电压前馈补偿为外环以电流控制为内环的控制系统,这种控制方式不仅能快速补偿电弧电压维持电弧稳定,而且双环控制能有效的减小系统误差,因此图 5 采用这种前馈补偿双闭环复合控制不仅可以保证系统的快速性和稳定性,而且有利于提高引弧率.

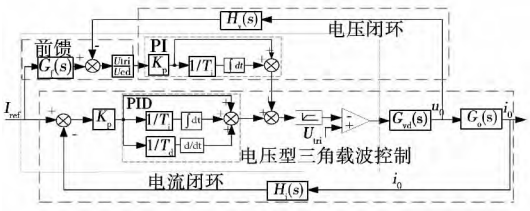

图 5　前馈补偿双闭环复合控制结构框图

Fig. 5　Composite control block of double closed-loop with feed-forward compensation

2　仿真及试验结果分析

2.1　控制策略仿真结果分析

通过对等离子静电弧及弧稳定性的分析,推导出等离子电弧数学模型,采用前馈补偿双闭环复合控制策略设计适用非高频引弧的数字化控制系统,并利用 Simulink 搭建等离子切割电源电路拓扑结构. 图 6 为电源非高频(LF)引弧过程、引弧转移至切割及弧能量突变过程的仿真结果. 结果表明,采用此新型的控制策略时,输出电流和输出电压能快速响应给定指令,具有良好的快速性和稳定性,仿真结果验证了控制策略的可行性和正确性.

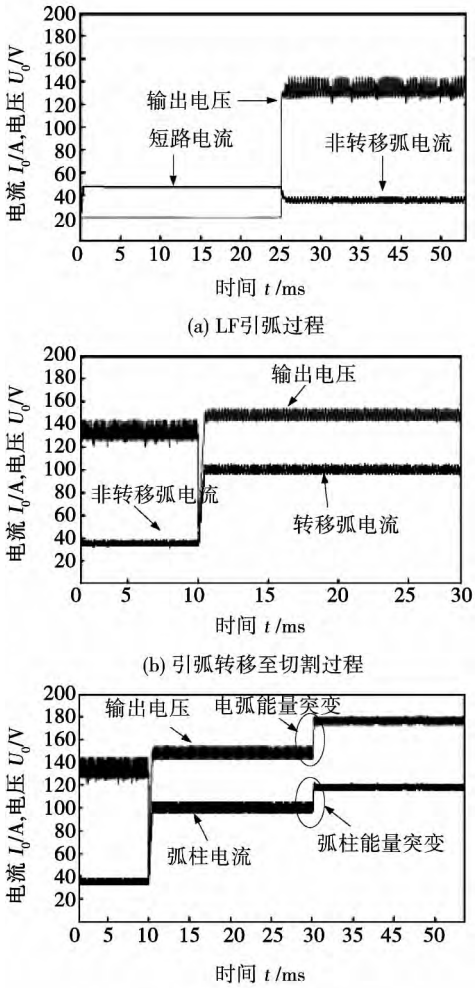

图 6　Simulink 仿真负载电流电压输出波形

Fig. 6　Output voltage and current waveforms of load by Simulink simulation

2.2　基于弧控制的新型复合控制系统试验结果分析

根据控制策略及仿真分析,以 TMS320F2808 为主控芯片,搭建 20 kW/100 A 试验样机. 图 7a 为等离子切割电源的非高频(LF)引弧过程,起弧前电极与喷嘴处于短路状态,设定引弧电流为 25 A,此时系统维持着 25 A 的短路电流,当引弧信号到来,则气路打开,在机械、热、电磁三者共同作用下形成了非转移弧. 此时引弧电流有跌落迹象,如果控制不佳

则会出现断弧，无法完成引弧. 系统通过电压前馈补偿快速建立引弧电压来维持电流稳定，减小跌落的程度，保持电弧电流稳定在 25 A，保证成功起弧，形成了稳定的非转移弧. 非转移弧稳定后，将喷嘴靠近工件，通过检测切割回路电流，当电流大于一定阈值时，将引弧信号置低，此时电弧由非转移弧切换至转移弧，由试验现象获知负载的变化会导致弧柱电压不稳定，因此此过程需具备良好的鲁棒性及快恢复性，试验过程中采用电压环补偿有效的解决了此问题，并能维持电压和电流恒定，如图 7b 所示，系统不仅快速跟随电流变化且迅速稳定，达到良好的控制效果. 图 7c 是在转移弧稳定后切割电流增加引起弧能量突变的过程中电流突增，切割电流快速跟随并稳定. 图 7d 是在板材切割时输出电流为 50 A 情况下系统达到了稳态，并具有良好的稳定性.

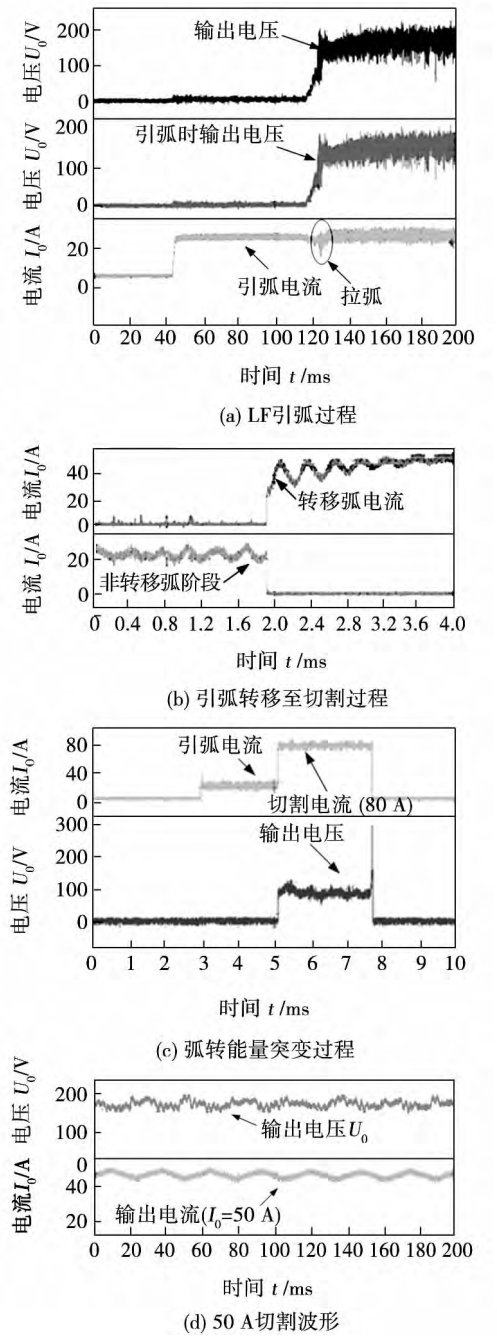

图 7 逆变式等离子切割电源样机试验波形

Fig. 7 Experimental waveforms of air plasma cutting inverter prototype

3 结 论

(1) 等离子电弧静态特性模型的建立，有利于对等离子电弧及电源的稳定性进行研究.

(2) 给定电流结合弧静态模型设计的电压前馈补偿方式有利于弧柱电压快速建立，提高非高频引弧的引弧率.

(3) 基于弧控制的新型复合控制策略，不仅具备良好的动态响应能力和鲁棒性能，也提高了电源的性能和切割质量.

参考文献:

[1] Narongrit Sanajit, Anuwat Jangwanitlert. Improved performance of a plasma cutting machine using a half-bridge DC/DC converter [C] // Robotics and Biomimetics, Bangkok, Thailand, 2009: 1601 – 1608.

[2] Sanajit N, Jangwanitlert A. A half-bridge DC/DC converter for plasma cutting machine [C] // Power Electronics and Drive Systems, Bangkok, Thailand, 2007: 1223 – 1227.

[3] Ramakrishnan S, Maya Gershenzon, Frederick Polivka, *et al*. Plasma generation for the plasma cutting process [J]. IEEE Translations on Plasma Science, 1997, 25(5): 937 – 946.

[4] Jia Deli, You Bo, Ren Wenbo, *et al*. Decoupling control based on PID neural network for plasma cutting system [C] // 27th Chinese Control Conference, Kunming, Yunnan, China, 2008: 659 – 662.

[5] Young Min Chae, Yungtaek Jang, Milan M, *et al*. A novel mixed current and voltage control scheme for inverter arc welding machines [C] // IEEE Applied Power Electronics Conference Exposition, Anaheim IEEE, China, 2001: 308 – 313.

[6] 刘宝其，段善旭，李 勋，等. 逆变式等离子切割电源双闭环控制策略 [J]. 中国电机工程学报，2011，31(9)：15 – 22.
Liu Baoqi, Duan Shanxu, Li Xun, *et al*. Double closed loop control strategy for plasma cutting inverter [J]. Proceedings of the CSEE, 2011, 31(9): 15 – 22.

[7] Nguyen Phi Long, Yasunori Tanaka, Yoshihiko Uesugi. Numerical investigation of the swirl gas angle and arc current dependence on evaporation of hafnium cathode in a plasma cutting arc [J]. Plasma Science, 2012, 40(2): 497 – 504.

[8] 雷玉成，郑惠锦. 工艺参数对焊接等离子弧的影响 [J]. 焊接学报，2001，22(6)：73 – 76.
Lei Yucheng, Zheng Huijin. Procedure parameters in plasma arc

welding [J]. Transactions of the China Welding Institution, 2011, 22(6): 73 - 76.

[9] Ramakrishnan S, Rogozinski M W. Properties of electric arc plasma for metal cutting [J]. Journal of Physics D: Applied Physics, UK, 1997, 30(4): 636 - 644.

[10] 殷凤良, 胡绳荪, 郑振太, 等. 等离子弧焊电弧的数值模拟 [J]. 焊接学报, 2006, 27(8): 51 - 54.
Yin Fengliang, Hu Shengsun, Zheng Zhentai, *et al*. Numerical simulation of plasma arc welding [J]. Transactions of the China Welding Institution, 2006, 27(8): 51 - 54.

[11] 戴朝波, 林海雪. 电压源型逆变器三角载波电流控制新方法 [J]. 中国电机工程学报, 2002, 22(2): 99 - 102.
Dai Chaobo, Lin Haixue. A noveltriangular carrier current control for voltage source inverters [J]. Proceedings of the CSEE, 2002, 22(2): 99 - 102.

[12] 朱国荣, 钱翠锋, 段善旭, 等. 逆变式焊/割电源滑模变结构与 PI 综合控制 [J]. 焊接学报, 2009, 30(2): 53 - 57.
Zhu Guorong, Qian Cuifeng, Duan Shanxu, *et al*. SMVSC and PI integrated control in inverter welding/cutting power [J]. Transactions of the China Welding Institution, 2009, 30(2): 53 - 57.

作者简介: 孙　强,男,1955 年出生,硕士,教授. 主要研究方向为现代高效功率变换器理论及应用. 发表论文 40 余篇. Email: sq@xaut.edu.cn

posite using Cu-25Sn-10Ti filler alloy. The interfacial microstructure of joint was analyzed and its formation mechanism was discussed, and also the impact of interfacial microstructure on shear strength of joints at different holding time was studied. Results show that continuous interfacial reaction layer has been formed at both sides of the base materials at brazing temperature 880 ℃ and holding time for 15 min, while the typical interfacial microstructure was Invar alloy/Fe_2Ti + Cu(s,s) + (Ni, Fe, Cu)$_2$TiSn/Cu(s,s) + $Cu_{41}Sn_{11}$ + CuTi/TiSi + Ti_2O_3/SiO_{2f}/SiO_2 composite. Holding time increasing would enlarge the thickness of TiSi Ti_2O_3 layer near SiO_{2f}/SiO_2 composite, and Fe_2Ti particles would turn into blocks. The shear strength of joint would also change with increasing of holding time. The shear strength of the joints reaches a maximum of 11.86 MPa when the temperature is 880 ℃ and the holding time is 15 min.

Key words: SiO_{2f}/SiO_2 composite; Invar alloy; brazing; interfacial microstructure; shear strength

In-situ observation of cracking in wollastonite coatings and effect of powder size on fracture WANG Lubin, WANG Weize, CHEN Yufan, XUAN Fuzhen (Key Laboratory of Pressure Systems and Safety, Ministry of Education, East China University of Science and Technology, Shanghai 200237, China). pp 57 – 60

Abstract: Fracture analysis of coatings has an important role on the investigation of coating's failure mechanism, the optimization of the processing parameters and the design. The fracture of plasma sprayed wollastonite coatings was observed in-situ by using a scanning electron microscope (SEM) during the tapered double cantilever beam (TDCB) specimens were pulled open. Additionally, the effect of powder size on the coating's fracture toughness is investigated based on the observation of the microstructure, fracture morphology and cracking propagation of coatings. It was found that the cracking path was mainly influenced by the applied stress. The original pores in the coatings, including the large pores, cracks and non-bounded interfaces could guide the cracking somewhat. The fracture toughness of coatings increased and fracture paths were more curved with the decreasing of powder size

Key words: coating fracture; in-situ observation; wollastonite; plasma spraying

Linear cumulative damage analysis of welded joints under combined cycle fatigue ZHANG Tao, WANG Dongpo, DENG Caiyan, WU Liangchen (School of Material Science and Engineering, Tianjin University, Tianjin 300072, China). pp 61 – 65

Abstract: 16Mn steel welded joints are tested to fail under low cycle fatigue, high cycle fatigue and combined cycle fatigue using an apparatus that is capable of providing interactive loading. A linear cumulative damage theory is used to estimate the fatigue life of the butt joints. The proportion of each of the two fatigue load components which cause the cumulative damage is calculated. The research indicate that high cycle fatigue loads and low cycle fatigue loads simply calculated as proportion would seriously underestimate the coupling between the two components of the fatigue load when we use Miner rule to calculate the fatigue cumulative damage of specimens. However, we can take into account of the coupling between the high and low cycle fatigue loads when we turn to the outsourcing envelope of the low cycle fatigue loads.

Key words: welded joints; combined cycle fatigue; linear cumulative damage

Characteristic of temperature distributions in stirring tools during friction stir welding LI Jingyong, ZHAO Yangyang, KANG Xiaoliang (Advanced Welding Technology Provincial Key Laboratory, Jiangsu University of Science and Technology, Zhenjiang 212003, China). pp 66 – 70

Abstract: The temperature distribution in stirring tools was measured by experimental method. It is shown that the characteristic of temperature distribution in stirring tools is much different from that in workpieces. At the beginning stage of friction stir welding, the softening in stirring zone reduces the friction coefficient and the friction heat between the stirring pin and the workpiece, so the temperature in stirring tools stops rising, whereas decreases in the exterior margin of the tool before the shoulder touches the workpiece. At the steady welding stage, equilibrium exists between the heat quantity delivered to and dissipated through the stirring tool, and its temperature keeps little fluctuation. The surface of the high-speed rotating tool has intensive heat exchange with the air around it, so the temperature near its axis is higher than that on the exterior margin. The stirring tools made of metal with lower specific heat capacity and higher coefficient of heat transfer lead to heat within the welding area dissipating faster.

Key words: friction stir welding; stirring tool; temperature field

A novel composite control strategy for plasma cutting power supply based on arc control SUN Qiang, CHEN Long, CHEN Guitao, WANG Huamin (Automation & Information Engineering College, Xi'an University of Technology, Xi'an 710048, China). pp 71 – 75

Abstract: This paper analyzes static characteristics of plasma arc with the derivation of plasma arc mathematical model according to the application of low-frequency(LF) pilot arc technology in the plasma cutting power supply, and integrates with the control requirements in low-frequency(LF) pilot arc, arc transferring and arc energy transferring, and proposes a novel composite control strategy. In order to meet the power's control requirements of rapidity and stability with the load of low-frequency(LF) pilot arc, the inner loop of this strategy builds up voltage loop composite control with feed-forward arc voltage and feedback arc voltage, and the current outer loop controls the energy of plasma arc, forming a control method of feed-forward composite control of double closed-loop. Simulations and experiments were given to verify that the mentioned control strategy not only improved system's stability and robustness, but also had excellent dynamic responsibility. The power had well non-liner resilience, meeting requirements for plasma cutting power supply.

Key words: plasma cutting power supply; arc control;

feed-forward compensator; feed-forward composite control of double closed-loop

Microstructure and wear behavior of Fe-based coating prepared by plasma transferred arc-welding YAO Haihua[1], ZHOU Zheng[1], HE Dingyong[1], ZHAO Qiuying[2], LI Ran[1] (1. College of Materials Science and Engineering, Beijing University of Technology, Beijing 100124, China; 2. Postdoctoral Research Station of Mechanical Engineering, Beijing University of Technology, Beijing 100124, China). pp 76 - 80

Abstract: A new Fe-based alloy powder was designed to prepare coatings by plasma transferred arc-welding (PTAW) process on AISI304L stainless steel substrate. The microstructure and wear behavior of the relative coating were detected by XRD, SEM and a rubber wheel abrasive testing machine respectively, in comparison with that of the traditional NiCrBSi and NiCrBSi + 25% WC coatings. The results show that the matrix of Fe-based coating consists of Fe-Cr solid solution and γ-Fe phase, surrounded by numerous dispersed Mo-rich borides and $M_{23}(B,C)_6$ hard phases, which contribute to support and strengthen the coating organization. The Fe-based coating exhibits high average hardness of 64.2 HRC, and excellent wear resistance which is better of that of the NiCrBSi + 25% WC coating and exceeds 8 times of that of the NiCrBSi coating.

Key words: plasma transferred arc-welding; Fe-based coating; microstructure; wear behavior

Effect of oxygen content on wettability and mechanical property of brazing seam for silver based powdered brazing filler metal ZHANG Guanxing[1], LONG Weimin[1], PAN Jianjun[1], LI Hao[2] (1. State Key Laboratory of Advanced Brazing Filler Metals and Technology, Zhengzhou Research Institute of Mechanical Engineering, Zhengzhou 450001, China; 2. School of Materials Science & Engineering, Zhengzhou University, Zhengzhou 450001, China). pp 81 - 84

Abstract: The properties of silver brazing filler metal with different oxygen content were studied by optical microscope, scanning electron microscopy and other analytical tools. The results of the experiment indicate that with the increase of oxygen content, the melting point of the solder alloy rises, which is 56 ℃ higher than that is casted when oxygen content is 0.6047%. With increase of the oxygen content, the surface layer of the brazing filler metal was covered with much oxide, the wetting ability between the solder and the substrate significantly decreases. When the oxygen content is about 0.02%, the tensile strength of the brazing filler metal is lowered slightly. When the oxygen content increases to more than 0.03%, the tensile strength decreases from over 300 MPa to about 170 MPa. The size of the inclusions in the welded joint increases with the oxygen content increases, while the brazed rate decreases.

Key words: oxygen content; wettability; tensile strength; oxide

Effect of thermal aging on intermetallic compounds and properties of Sn-Cu-Ni-xPr/Cu soldered joints MA Chaoli[1], XUE Songbai[1], LI Yang[1], XU Yiwei[1], JIANG Junyi[2] (1. College of Materials Science and Technology, Nanjing University of Aeronautics and Astronautics, Nanjing 210016, China; 2. Jinhua Shuanghuan Brazing Alloys Co., Ltd, Jinhua 321000, China). pp 85 - 88

Abstract: Chip resistors were joined with Sn-0.7Cu-0.05Ni-xPr solder. To guarantee the reliability of the Sn-0.7Cu-0.05Ni-xPr/Cu joints in service requirement, the growth rate of intermetallic compounds of Cu side was evaluated and the effects of the intermetallic compound layer on the electrical and mechanical properties have been investigated under various aging time. The shear strength of Sn-0.7Cu-0.05Ni-xPr/Cu joint gradually decreased during thermal aging. Meanwhile, under the same condition, the Sn-0.7Cu-0.05Ni-xPr/Cu joint achieved good mechanical properties when the addition of Pr was about 0.05%.

Key words: lead free solder; thermal aging; interface thickness; mechanical properties

Effects of boron on microstructures and wear resistance of Fe-Cr-C system hardfacing alloys ZHANG Yanchao, CUI Li, HE Dingyong, ZHOU Zheng (College of Materials and Science Engineering, Beijing University of Technology, Beijing 100124, China). pp 89 - 92, 104

Abstract: Fe-Cr-C based hardfacing alloys were produced by the CO_2 gas shielded welding process utilizing the flux cored wires of 1.6 mm in diameter on low-carbon steel substrates. The hardfacing alloys contained the carbon contents in the range of 1.0%-3.0%, chromium contents of 15%-25%, boron contents of 0%-2.0%. The effects of boron carbide contents on the microhardness and wear resistance of the hardfacings were studied. The results show that the hardness increased from 57.1 HRC to 65.2 HRC as the boron contents reaches up to 2.0%. Compared without boron addition, the hardness increases by 14.2% times. The relative wear resistance increases from 3.5 to 18.0 times. By using of the optical microscope (OM), scanning electron microscope (SEM) and X-ray diffraction (XRD), the microstructures and distribution of carbides in the matrix were investigated. The microstructures of metallic matrix are composed by ferrite, austenite, $(Fe,Cr)_7C_3$, Fe_2B, etc. The additions of boron carbide in the wires can improve the microstructure of the matrix of the hardfacing alloys and the quantities of the carbides. The distribution of $(Fe,Cr)_7C_3$ particles are uniformly dispersed.

Key words: Fe-Cr-C hardfacing alloys; flux cored wires; microstructures; wear resistances

Effect of heat inputs on low temperature toughness of F550Z steel welding joints YAN Keng, YE Fengyu, LIU Wei (Provincial Key Lab of Advanced Welding Technology, Jiangsu University of Science Technology, Zhenjiang 212003, China). pp 93 - 96

Abstract: Effect of different heat inputs on microstructure and low temperature toughness of 550 Mpa offshore steel welding joints was studied. The experimental results indicate when the heat input is 15 kJ/cm or 50 kJ/cm, the welding metal experience the effect of heat treatment, and the microstructures are acicular ferrite and fine granular dispersed carbides, especially when the heat input is 50 kJ/cm. In the impact test at -60 ℃,